J|A|C|S
ARTICLES
Published on Web 01/31/2004

Dynamic Nature of the Intramolecular Electronic Coupling Mediated by a Solvent Molecule: A Computational Study

Alessandro Troisi,*,† Mark A. Ratner,† and Matthew B. Zimmt‡

Contribution from the Department of Chemistry, Materials Research Center and Center for Nanofabrication and Molecular Self-Assembly, Northwestern University, Evanston, Illinois, and Department of Chemistry, Brown University, Providence, Rhode Island

Received October 6, 2003; E-mail: troisi@ciam.unibo.it

Abstract: We present a combined Molecular Dynamics/Quantum Chemical study of the solvent-mediated electronic coupling between an electron donor and acceptor in a C-clamp molecule. We characterize the coupling fluctuations due to the solvent motion for different solvents (acetonitrile, benzene, 1,3-diisopropylbenzene) for the charge separation and the charge recombination processes. The time scale for solvent-induced coupling fluctuation is ~0.1 ps. The effect of these fluctuations on the observed rate is discussed using a recently developed theoretical model. We show that, while the microscopic charge transfer process is very complicated and its computational modeling very subtle, the macroscopic phenomenology can be captured by the standard models. Analyzing the contribution to the coupling given by different solvent orbitals, we find that many solvent orbitals mediate the electron transfer and that paths through different solvent orbitals can interfere constructively or destructively. A relatively small subset of substrate−solvent configurations dominate contributions to solvent-mediated coupling. This subset of configurations is related to the electronic structure of the C-clamp molecule.

Introduction

The charge transfer (CT) reaction in donor−bridge−acceptor systems is one of the most extensively studied processes in chemistry. The early theories[1] beautifully account for the kinetic data in simple systems[2] and still form the basis for the present understanding of the CT.[3] However, with the increasing complexity of the systems under investigation, the phenomenology has become richer and the many new issues justify the apparently inexhaustible interest in this area.

One common feature of many recent studies is the increased importance attributed to the dynamics of the bridge. In several systems the bridge undergoes conformational changes that alter the CT rate constant, leading to what is sometimes called *conformational gating*, i.e., the control of the electron motion by the nuclear degrees of freedom of the bridge.[4−8] In the limit of slow conformational changes, the overall kinetics in these cases may be nonexponential.[9] When the bridge conformational changes influence the electronic coupling and occur on faster time scales, the system experiences a breakdown of the Condon approximation[10−12] that may lead to an anomalous temperature dependence of the rate constant, as found experimentally for example by Davis[13] and discussed theoretically by several authors. In other systems, electronic states with a net charge on the bridge may be thermally populated leading to the incoherent mechanism of CT, which has received much attention in the past year both theoretically[14−17] and experimentally.[18,19]

Together with phenomenological theories, the interpretation of the CT experimental data has been assisted by molecular modeling techniques. These methods, which have been tradi-

* Corresponding author. Current address: Dipartimento di Chimica "G. Ciamician", Universita' di Bologna, via Selmi 2, 40126, Bologna, Italy.
† Northwestern University.
‡ Brown University.

(1) (a) Marcus, R. A. *J. Chem. Phys.* **1956**, *24*, 966. (b) Hush, N. S. *Trans. Faraday Soc.* **1961**, *57*, 557. (c) Jortner, J. *J. Chem. Phys.* **1976**, *64*, 4860.
(2) Closs, G. L.; Miller, J. R. *Science* **1988**, *240*, 440.
(3) (a) Bixon, M.; Jortner, J. *Adv. Chem. Phys* **1999**, *106*, 35. (b) Newton, M. D. *Adv. Chem. Phys* **1999**, *106*, 303. (c) A. Nitzan, *Ann. Rev. Phys. Chem.* **2001**, *52*, 681.
(4) Brunschwig, B. S.; Sutin, N. *J. Am. Chem. Soc.* **1989**, *111*, 7454.
(5) Kuila, D.; Natan, M. J.; Rogers, P.; Gingrich, D. J.; Baxter, W. W.; Arnone, A.; Hoffman, B. M. *J. Am. Chem. Soc.* **1991**, *113*, 6520.
(6) Graige, M. S.; Feher, G.; Okamura, M. Y. *Proc. Natl. Acad. Sci. U.S.A.* **1998**, *95*, 11679.
(7) (a) Henderson, P. T.; Jones, D.; Hampikian, G.; Kan, T. Z.; Schuster, G. B. *Proc. Nat. Acad. Sci. U.S.A.* **1999**, *96*, 8353. (b) Sanii, L.; Schuster, G. B. *J. Am. Chem. Soc.* **2000**, *122*, 11545. (c) Barnett, R. N.; Cleveland, C. L.; Joy, A.; Landman, U.; Schuster, G. B. *Science* **2001**, *294*, 567.
(8) (a) Ratner, M. A. *Proc. Natl. Acad. Sci. U.S.A.* **2001**, *98*, 387. (b) Berlin, Y. A.; Burin, A. L.; Siebbeles, L. D. A.; Ratner M. A. *J. Phys. Chem. A* **2001**, *105*, 5666.
(9) (a) Cao, J. S. *Chem. Phys. Lett.* **2000**, *327*, 38. (b) Yang, S. L.; Cao, J. S. *J. Phys. Chem. B* **2001**, *105*, 6536.
(10) Ratner, M. A.; Madhukar, A. *Chem. Phys.* **1978**, *30*, 201.
(11) Beratan, D. N.; Hopfield, J. J. *J. Chem. Phys.* **1984**, *81*, 5753.
(12) Mikkelsen, K. V.; Ratner, M. A. *J. Phys. Chem.* **1989**, *93*, 1759.
(13) Davis, W. B.; Ratner, M. A.; Wasielewski, M. R. *J. Am. Chem. Soc.* **2001**, *123*, 7877.
(14) (a) Felts, A. K.; Pollard, W. T.; Friesner, R. A. *J. Phys. Chem.* **1995**, *99*, 2929. (b) Pollard, W. T.; Felts, A. K.; Friesner, R. A. *Adv. Chem. Phys.* **1996**, *93*, 77.
(15) (a) Skourtis, S. S.; Mukamel, S. *Chem. Phys.* **1995**, *197*, 367. (b) Okada, A.; Chernyak, V.; Mukamel, S. *J. Phys. Chem. A* **1998**, *102*, 1241.
(16) (a) Segal, D.; Nitzan, A.; Ratner, M. A.; Davis, W. B. *J. Phys. Chem. B* **2000**, *104*, 2709. (b) Segal, D.; Nitzan, A.; Davis, W. B.; Wasielewski, M. R.; Ratner, M. A. *J. Phys. Chem. B* **2000**, *104*, 3817.
(17) (a) Berlin, Y. A.; Burin, A. L.; Ratner, M. A. *J. Am. Chem. Soc.* **2001**, *123*, 260. (b) Berlin, Y. A.; Hutchison, G. R.; Rempala, P.; Ratner, M. A.; Michl, J. *J. Phys. Chem. A* **2003**, *107*, 3970.
(18) Meggers, E.; Michel-Beyerle, M. E.; Giese, B. *J. Am. Chem. Soc.* **1998**, *120*, 12950.
(19) Schlag, E. W.; Lin, S. H.; Weinkauf, R.; Rentzepis, P. M. *Proc. Natl. Acad, Sci. U.S.A.* **1998**, *95*, 1358.

tionally used to provide alternative estimates of key quantities such as electronic coupling[20−23] and reorganization energies,[3b,24,25] are now often employed to investigate quantitatively the dynamics of the bridge and to evaluate its impact on the observed rate. In most of these studies a classical molecular dynamics (MD) simulation is coupled to a quantum chemical (QC) evaluation of the electronic coupling.[26−33] Adopting this approach, several recent papers investigated systems such as the azurin protein,[26,27] the photosynthetic system,[28] and DNA.[29] The main advantage of joining experimental studies with a computational investigation in this context is that the role of each individual factor (internal and external reorganization energy, electronic coupling, etc.) that contributes to the rate can be analyzed separately and the inaccuracy of the computed value does not affect the computation of other parameters. Given a model and a set of experimental measures, there are often many sets of parameters that lead to an agreement between the model and the experiment,[34] sometimes leaving doubts as to the correct interpretation.

We present here a computational study of the electron-transfer mediated by a solvent molecule in a C-shaped D−B−A compound (denoted as A9DME) synthesized[35] and extensively studied by Zimmt and co-workers[36−41] (see Figure 1). Molecules with the same topology also have been studied by Paddon−Row and co-workers.[42]

In this system, D and A are kept at a distance of ca. 7 Å by a curved saturated bridge. The DA distance and the configuration of the bridge make the electron transfer through space (i.e., through the molecular cavity) more probable than through bond. However, the solvent can substantially lower the barrier for

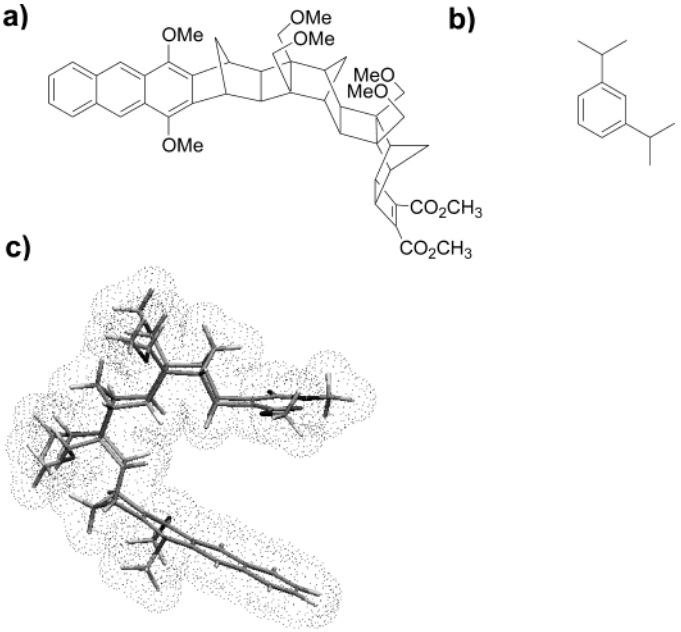

Figure 1. (a) C-Clamp molecule under investigation and (b) 1,3-diisopropylbenzene (1,3-DIB), one of the three solvents, together with MeCN and benzene, considered in this work. (c) Representation of the solvent-accessible region of the solute.

electron tunneling between D and A and its role in mediating charge transfer has been examined in several studies.[36−38] This system provides an excellent case for integration of computational models and interpretation of experimental data. The potential role of the solvent in the charge transport process was proposed theoretically[43] before its first experimental verification.[36] Afterward, the modeling of the experimental data took advantage of the numerical evaluation of the reorganization energy through the Poisson−Boltzmann equations and independent estimates of the coupling strength with ab initio and semiempirical techniques.[44] As expected, the concavity makes the actual size of the solvent molecule very important for the reorganization energy, and a more sophisticated model, accounting for the discontinuous nature of the solvent, was employed to reproduce the temperature dependence of the reorganization energy.[39,45]

An aspect that has not been investigated and constitutes the subject of this paper is the role of solvent *dynamics* in the DA coupling. The situation is reminiscent of CT reactions mediated by fluctuating bridges, except that here the bridging medium is the solvent. This situation leads to the maximization of non-Condon effects, as the coupling is expected to be extremely dependent on the solvent configuration. The fitting of experimental data, done while neglecting non-Condon effects, gives an *effective electronic coupling* value that may reflect many possibilities: the solvent can sit in few preferential positions, enter or exit from the cavity, or sample almost uniformly the free volume inside the cavity. To assess the effect of solvent motions on the measured rate it is not sufficient to compute only the distribution function of the solvent around the molecule because it is also the *time scale* of the solvent motions that

(20) Ratner, M. A. *J. Phys. Chem.* **1990**, *94*, 4877.
(21) Priyadanshy, S.; Risser, S. M.; Beratan, D. N. *J. Phys. Chem.* **1996**, *100*, 17678.
(22) Skourtis, S. S.; Beratan, D. N. *Adv. Chem. Phys.* **1999**, *106*, 377.
(23) Cave, R. J.; Newton, M. D. *Chem. Phys. Lett.* **1996**, *249*, 15.
(24) Tomasi, J.; Persico, M. *Chem. Rev.* **1994**, 94, 2027.
(25) Jakobsen, S.; Mikkelsen, K. V.; Pedersen, S. U. *J. Phys. Chem.* **1996**, *100*, 7411.
(26) Daizadeh, I.; Medvedev, E. S.; Stuchebrukhov, A. A. *Proc. Natl. Acad. Sci.* **1997**, *94*, 3703.
(27) (a) Xie, Q.; Archontis, G.; Skourtis, S. S.; *Chem. Phys. Lett*. **1999**, *312*, 237. (b) Skourtis, S. S.; Archontis, G.; Xie, Q. *J. Chem. Phys.* **2001**, *115*, 9444.
(28) Balabin, I. A.; Onuchic, J. N. *Science* **2000**, *290*, 114.
(29) Troisi, A.; Orlandi, G. *J. Phys. Chem. B* **2002**, *106*, 2093.
(30) (a) Schlag, E. W.; Sheu, S. Y.; Yang, D. Y.; Selzle, H. L.; Lin, S. H.; *Proc. Nat. Acad. Sci. U.S.A.* **2000**, *97*, 1068. (b) Schlag, E. W.; Yang, D. Y.; Sheu, S. Y.; Selzle, H. L.; Lin, S. H.; Rentzepis, P. M. *Proc. Natl. Acad. Sci. U.S.A.* **2000**, *97*, 9849.
(31) Jones, G. A.; Paddon-Row: M. N.; Carpenter, B. R.; Piotrowiak, P. *J. Phys. Chem. A* **2002**, *106*, 5011.
(32) Miller, N. E.; Wander, M. C.; Cave, R. J. *J. Phys. Chem. A* **1999**, *103*, 1084.
(33) Castner, E. W.; Kennedy, D.; Cave, R. J. *J. Phys. Chem. A* **2000**, *104*, 2869.
(34) Napper, A. M.; Read, I.; Waldeck, D. H.; Kaplan, R. W.; Zimmt, M. B. *J. Phys. Chem. A* **2002**, *106*, 4784.
(35) Kumar, K.; Tepper, R.; Zeng, Y.; Zimmt, M. B. *J. Org. Chem.* **1995**, *60*, 4051.
(36) (a) Kumar, K.; Lin, Z.; Waldeck, D. H.; Zimmt, M. B. *J. Am. Chem. Soc.* **1996**, *118*, 243. (b) Han, J.; Zimmt, M. B. *J. Am. Chem. Soc.* **1998**, *120*, 8001.
(37) Kaplan, R.; Napper, A. M.; Waldeck, D. H.; Zimmt, M. B. *J. Am. Chem. Soc.* **2000**, *122*, 12039.
(38) Vath, P.; Zimmt, M. B.; Matyushov, D. V.; Voth, G. A. *J. Phys. Chem. B* **2000**, *103*, 9130.
(39) Kaplan, R.; Napper, A. M.; Waldeck, D. H.; Zimmt, M. B. *J. Phys. Chem. A* **2002**, *106*, 1917.
(40) Napper, A. M.; Read, I.; Kaplan, R. W.; Zimmt, M. B.; Waldeck, D. H. *J. Phys. Chem. A* **2002**, *106*, 5288.
(41) Zimmt, M. B.; Waldeck, D. H. *J. Phys. Chem. A* **2003**, *107*, 3580.
(42) (a) Lokan, N. R.; Paddon-Row, M. N.; Koeberg, M.; Verhoeven, J. W. *J. Am. Chem. Soc.* **2000**, *122*, 5075. (b) Napper, A. M.; Head, N. J.; Oliver, A. M.; Shephard, M. J.; Paddon-Row: M. N.; Read, I.; Waldeck, D. H. *J. Am. Chem. Soc.* **2002**, *124*, 10171.
(43) Cave, R. J.; Newton, M. D.; Kumar, K.; Zimmt, M. B. *J. Phys. Chem.* **1995**, *99*, 17501.
(44) Kumar, K.; Kurnikov, I. V.; Beratan, D. N.; Waldeck, D. H.; Zimmt, M. B. *J. Phys. Chem. A* **1998**, *102*, 5529.
(45) Matyushov, D. V. *Chem. Phys.* **1993**, *174*, 199.

determines the observed kinetics.[9,46,48] Moreover, it is necessary to include explicitly the liquid medium surrounding the molecule, because the geometry of the solvent inside the cavity is also determined by the solvent−solvent interaction. In this paper, we use molecular dynamics (MD) simulations, based on an empirical force field, coupled with a quantum chemical (QC) evaluation of the electronic coupling between donor and acceptor to characterize the time dependence of the electronic coupling through solvent. We used a recently developed theoretical model to evaluate the effect of the computed coupling dynamics on the CT process.[48]

Besides the initial motivation, the MD/QC analysis also provides insight into several other aspects of the CT mechanism, including the potential role of multiple solvent molecules and the relevance of each solvent orbital. The analysis of the MD trajectories with different solvents can help discriminate between the common features of through-solvent CT and the unique characteristic of each solvent, providing hints for future generalizations.

2. Computational and Theoretical Methods

In A9DME, the donor is the dimethoxyanthracene chromophore whose lowest excited state Ψ^{LE}, obtained by irradiation at ∼375 nm, correlates with the L_a state of anthracene.[49] The charge transfer state, Ψ^{CT}, is in equilibrium with Ψ^{LE} and can decay nonradiatively to the ground state Ψ^0. In this paper, we will mainly focus on the charge separation (CS) process of the A9DME molecule in acetonitrile (MeCN) and consider for comparison the same process in benzene and 1,3-diisopropylbenzene (1,3-DIB). Experimental measurements are available for the three solvents, representative of a wide range of polarities and self-diffusion coefficients. In the case of MeCN, we will also consider the charge recombination (CR) process.

Force Field and MD Simulations. The original MM3[50] force field was employed to generate most of the MD trajectories.[51,52] It was selected because of the good results obtained for isolated conjugated molecules and supramolecular assemblies governed by $\pi-\pi$ stacking.[53] To build the starting geometry for the simulation, a 20 × 20 × 20 Å cube of each solvent at standard density was equilibrated at 300 K with periodic boundary conditions. The solute was placed in the middle of several replicas of this cube, and solvent molecules within the van der Waals radius of the solute atoms were eliminated. Finally, the simulation box around the solute was defined so that the minimum distance between solute atoms in two different images was 24 Å (leading to a box of c.a. 39 × 39 × 39 Å). The number of solvent molecules was 534, 272, and 154 for MeCN, benzene, and 1,3-DIB, respectively. The energy of the system was minimized, and from this geometry, a 50 ps equilibration dynamics at the desired temperature led to the starting trajectory point for the production dynamics. MD calculations were run at a constant temperature within the canonical ensemble using the Berendsen[54] algorithm. Hydrogen atoms were constrained at their ideal bond distance using the RATTLE algorithm[55] while the remaining degrees of freedom were left flexible. The integration time step was 2 fs. The length of each trajectory was in the 500−1000 ps range, and the interval between QC calculations was in the 2−40 fs range (see also Table 1).

Table 1. Number of Occupied and Virtual Orbitals Considered for the Various Solvent Molecules, the Energy Difference ΔE between the Highest and Lowest Orbital Considered, the Energy of the HOMO and the LUMO of the Solvent Molecule Inside the Cavity, and the Tunneling Energy for the Charge Separation and Recombination Processes[a]

solvent	$N_{occ} + N_{virt}$	ΔE	$E_{solv-HOMO}$	$E_{solv-LUMO}$	E_{tunn} (CS)	E_{tunn} (CR)
MeCN	6 + 7	1.2	−0.4262	0.0640	−0.0358	−0.1558
benzene	9 + 12	0.97	−0.3327	0.0359	−0.0640	
1−3DIB	20 + 26	1.0	−0.3126	0.0389	−0.0354	

[a] Energies were averaged over the MD trajectories and are listed in atomic units.

We also performed two simulations of the charge separated (D+)−(A−) state, at which point charges were added to the donor and acceptor atoms, leaving all the other parameters unchanged. To find the additional charges we first computed the optimal point charges that reproduce the electrostatic potential around the molecule using the CHELPG scheme[56] and ab initio calculations at the (U)HF/6-31G(d) of the species D, D+, A, and A− (at the optimized geometry of the neutral species). The differences in point charge distributions between D+ and D and between A− and A give the partial charge to be added to each atom in order to reproduce the electrostatic change that follows the CT process. This approach, often used in the extension of MM3 force field,[57] gave good quantitative results[58] and should describe correctly the attraction between the D+ and A− fragments and the solvent−solute interaction. Since MM3 is a nonpolarizable force field, the simulations of the charge-separated species were carried out only for the MeCN solvent whose interactions with the charged solute are mainly of the dipole−charge type.

QC Calculations: Hamiltonian and Effective Coupling Calculation. The INDO/S Hamiltonian[59,60] was used to perform the QC calculation because it provides the best compromise between accuracy and speed. The reliability of INDO/S for the calculation of interorbital couplings was demonstrated many times,[61] and since our simulations require several millions of QC calculations at different geometries, ab initio or density functional-type methods are not reasonable. Alternatively, one could reparametrize[29] or calibrate[32] the semiempirical methods with a subset of more accurate calculations.

Several theoretical[43] and experimental[36,37] considerations suggest that the coupling provided by pathways through the saturated C-shaped bridge is negligible with respect to the direct (through space or solvent) D−A coupling. We therefore limited our QC calculations to the subsystem illustrated in Figure 2 containing three nonbonded fragments: D, A, and S (solvent). For each snapshot of the MD trajectory, the atomic coordinates of the three fragments are extracted and used for the QC calculation (after saturating the dangling bonds with

(46) Tang, J. *J. Chem. Phys.* **1993**, *98*, 6263.
(47) Medvedev, E. S.; Stuchebrukhov, A. A. *J. Chem. Phys.* **1997**, *107*, 3821.
(48) Troisi, A.; Nitzan, A.; Ratner, M. A. *J. Chem. Phys.* **2003**, *119*, 5782.
(49) Michl, J.; Thulstrup, E. W. *Spectroscopy with Polarized Light*; New York, VCH: New York, 1986; p 405.
(50) (a) Allinger, N. L.; Yuh, Y. H.; Lii, J.-H. *J. Am. Chem. Soc.* **1989**, *111*, 8551. (b) Allinger, N. L.; Li, F.; Yan, L.; Tai, J. C. *J. Comput. Chem.* **1990**, *11*, 868.
(51) (a) Cheatman, T. E.; Kollman, P. E. *Annu. Rev. Phys. Chem.* **2000**, *51*, 435. (b) Ravishanker, G.; Auffinger, P.; Langley, D. R.; Bhyravabhotla, J.; Matthew, A. Y.; Beveridge, D. L. *Rev. Comput. Chem.* **1997**, *11*, 317.
(52) MM3 calculations were performed with the TINKER suite of programs: (a) Dudek, M. J.; Ponder, J. W. *J. Comput. Chem.* **1995**, *16*, 791. (b) Kundrot, C. E.; Ponder, J. W.; Richards, F. M. *J. Comput. Chem.* **1991**, *12*, 402. (c) Ponder, J. W.; Richards, F. M. *J. Comput. Chem.* **1987**, *8*, 1016.
(53) (a) Gonzales, C.; Lim, E. C. *J. Chem. Phys. A* **1999**, *103*, 1437. (b) Georgakilas, V.; Pellarini, F.; Prato, M.; Guldi, D. M.; Melle-Franco, M.; Zerbetto, F. *Proc. Natl. Acad. Sci. U.S.A.* **2002**, *99*, 5075. (c) Leon, S.; Leigh, D. A.; Zerbetto, F. *Chem.−Eur. J.* **2002**, *8*, 4854.
(54) Berendsen, H. J. C.; Postma, J. P. M.; van Gunsteren, W. F.; Di Nola, A.; Haak, J. R. *J. Chem. Phys.* **1984**, *81*, 3684.
(55) Andersen, H. C. *J. Comput. Phys.* **1983**, *52*, 24.
(56) Breneman, C. M.; Wiberg, K. B. *J. Comput. Chem.* **1990**, *11*, 361.
(57) (a) Felder, C.; Jiang, H. L.; Zhu, W. L.; Chen, K. X.; Silman, I.; Botti, S. A.; Sussman, J. L. *J. Phys. Chem. A* **2001**, *105*, 1326. (b) Sorensen, J. B.; Lewin, A. H.; Bowen, J. P. *J. Mol. Struct. (THEOCHEM)* **2003**, *623*, 145. (c) Kirshner, K. N.; Lewin and A. H., Bowen, J. P. *J. Comput. Chem.* **2003**, *24*, 111.
(58) Zwier, J. M.; Brouwer, A. M.; Buma, W. J.; Troisi, A.; Zerbetto, F. *J. Am. Chem. Soc.* **2002**, *124*, 149.
(59) Pople, J. A.; Beveridge, D. L. *Approximate Molecular Orbital Theory*; McGraw-Hill: New York, 1970).
(60) Ridley, J. E.; Zerner, M. C. *Theor. Chim. Acta* **1973**, *32*, 111.
(61) Hill, I. G.; Kahn, A.; Cornil, J.; dos Santos, D. A.; Bredas, J. L. *Chem. Phys. Lett.* **2000**, *317*, 444.

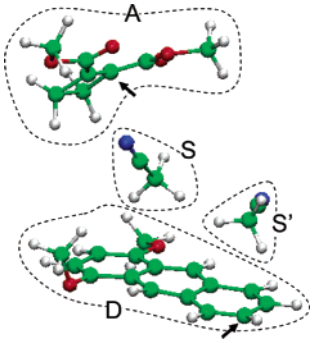

Figure 2. The fragments included in the quantum chemical calculation. S and S′ correspond to the first and second solvent molecule closest (based on center of mass) to the center of the cavity. The latter is the middle point between the two atoms identified by the small black arrows.

hydrogen). The solvent molecule most probably involved in the coupling was selected on a geometrical basis as the one with its center of mass closest to the center of the cavity (defined as in the caption of Figure 2). Since, in principle, more than one molecule can be involved, the second closest solvent molecule to the cavity center (S′) was also considered and the coupling calculation repeated for the triad D, A, S′ (possible interference effects and role of other solvent molecules will be discussed in Section 3).

Because of near-degeneracies along the trajectories, we could not use the generalized Mulliken−Hush analysis[23] to find the diabatic electronic state mixing.[62] The simple alternative we choose is to compute directly the coupling between the diabatic orbitals involved in the charge transfer.[63,64] The diabatic (or unperturbed) orbitals are naturally defined as the Hartree−Fock orbitals of the noninteracting fragments, and the diabatic states are linear combinations of configurations built on these diabatic orbitals. The Fock matrix elements F_{ij} between the orbitals of the D, A, and S fragments are computed in this diabatic basis. The orbitals of the D and A fragments are coupled directly (through-space coupling) and through the intervening solvent molecular orbitals. The effective coupling between D and A orbitals can be obtained from the full Fock matrix through a partitioning technique.[65,66] The full orbital space is divided into two subspaces: the DA subspace containing only the D and A orbitals, and the S subspace containing the solvent orbitals. The partitioned Fock matrix is:

$$\mathbf{F} = \begin{bmatrix} \mathbf{F}_{DA,DA} & \mathbf{F}_{DA,S} \\ \mathbf{F}_{S,DA} & \mathbf{F}_{S,S} \end{bmatrix} \quad (1)$$

An effective Fock matrix for the DA subspace can be written as:

$$\mathbf{F}_{DA}{}^{eff}(E_{tun}) = \mathbf{F}_{DA,DA} + (\mathbf{F}_{DA,S} - E_{tun}\mathbf{S}_{DA,S})(E_{tun}\mathbf{S}_{S,S} - \mathbf{F}_{S,S})^{-1} \times (\mathbf{F}_{S,DA} - E_{tun}\mathbf{S}_{S,DA}), \quad (2)$$

where the first and second terms correspond to the through-space and through-solvent components of the orbital coupling. **S** is the overlap matrix, and the parameter E_{tun} is set to the average value of the two orbitals between which the electron is exchanged.[66]

A CI calculation on the isolated DA system indicates that the states Ψ^{LE} and Ψ^{CT} are both described appropriately by a single electronic configuration corresponding to the excitation of an electron from the HOMO of D (φ_{DH}) to the LUMO of D (φ_{DL}) and to the LUMO of A (φ_{AL}), respectively.

$$\Psi^{LE} = \Phi_{DH\rightarrow DL} \quad (3)$$

$$\Psi^{CT} = \Phi_{DH\rightarrow AL} \quad (4)$$

Two orbital couplings are needed ($F^{eff}_{DH,AL}$ and $F^{eff}_{DL,AL}$) to compute the interstate coupling according to the Slater rules applied to the singlet spin-adapted configurations.[67] Using V^{CS} and V^{CR} to indicate the coupling matrix elements for charge separation and recombination and using the standard formalism for two-electron matrix elements, we arrive at the following equations:

$$V^{CS} = \langle Y^{LE}|H|\Psi^{CT}\rangle = F_{DL,AL}{}^{eff} + 2(\varphi_{DL}\varphi_{AL}|\varphi_{DH}\varphi_{DH}) - (\varphi_{DL}\varphi_{DH}|\varphi_{AL}\varphi_{DH}) \quad (5)$$

$$V^{CR} = \langle \Psi^0|H|\Psi^{CT}\rangle = \sqrt{2}F_{DH,AL}{}^{eff} \quad (6)$$

General eqs 2, 5, and 6 are further simplified by the INDO approximation:[59] the S matrix in eq 2 is unity, and the two-electron integrals in eq 5 are set to zero.

In the idealized C_s symmetry, Ψ^0 and Ψ^{CT} transform as the A′ representation, while Ψ^{LE} transforms as A″. In the symmetric conformation, CS is an electronically forbidden process, while the CR process is allowed. The most important symmetry-breaking perturbation that makes the CS process possible is provided by solvent molecules positioned asymmetrically in the clamp.[68]

Although it is often assumed that only the frontier orbitals of the bridging medium contribute to the superexchange mechanism, in this study we included a broad orbital window of the solvent in the cavity, to identify the orbitals that preferentially mediate the electron transfer. Table 1 lists the number of orbitals included for each solvent, the energy difference between the lowest and the highest orbitals considered, and the energy of the HOMO and the LUMO. We used the orbital energies of the ground state, although the orbital energies rigorously depend on the considered electronic state.

An overview of the MD simulations and the subsequent QC analysis that will be presented in this paper is given in Table 2. Simulations I−VI with MeCN solvent differ in the temperature, the time interval between QC calculations of the coupling, and the nature of the CT process attending the coupling (V^{CS} or V^{CR}). We used simulations of the neutral D−A molecule to compute V^{CS} and simulations of the charge

Table 2. Summary of the MD Simulations for Charge Separation (CS) and Charge Recombination (CR) Processes[a]

	solvent	type	temperature (K)	length (ps)	interval between QC calculations (ps)
I	MeCN	CS	260	500	0.002
II	MeCN	CS	300	500	0.002
III	MeCN	CS	360	500	0.002
IV	MeCN	CR	300	500	0.002
V	MeCN	CS	300	1000	0.01
VI	MeCN	CR	300	1000	0.01
VII	Benzene	CS	300	500	0.01
VIII	1−3DIB	CS	300	500	0.04

[a] Simulations I−IV are used to compute the function $\langle V(t)V(0)\rangle$ (note that a higher time resolution in the calculation of the coupling is needed). Simulations V and VI give the most extensive data for analyzing the coupling in MeCN. Simulations with benzene and DIB (VII and VIII) are used mainly for comparison to the MeCN results.

(62) Since the CT state is shifted to higher energy in the gas-phase calculations, electronic states that are otherwise irrelevant disturb the calculation. The multistate GMH cannot be used either, because it gives an unwanted complete mixing between the excited (non-CT) states and the ground state.
(63) Voityuk, A. A.; Rösch, N.; Bixon, M.; Jortner, J. *J. Phys. Chem. B* **2000**, *104*, 9740.
(64) Troisi, A.; Orlandi, G. *Chem. Phys. Lett.* **2001**, *344*, 509.
(65) Lowdin, P. O. *J. Math. Phys.* **1962**, *3*, 969.
(66) Priyadarshy, S.; Skourtis, S.; Risser, S. M.; Beratan, D. N. *J. Chem. Phys.* **1996**, *104*, 9673.
(67) Szabo, A.; Ostlund, N. S. *Modern Quantum Chemistry*; McGraw-Hill: New York, 1989.
(68) We note, in addition, that not even the "average" conformation of our molecule is rigorously of C_s symmetry, since the conformations of the ester groups within A are not mirror-symmetric, in the most stable conformation (from preliminary ab initio calculations on the A fragment) shown in Figure 2.

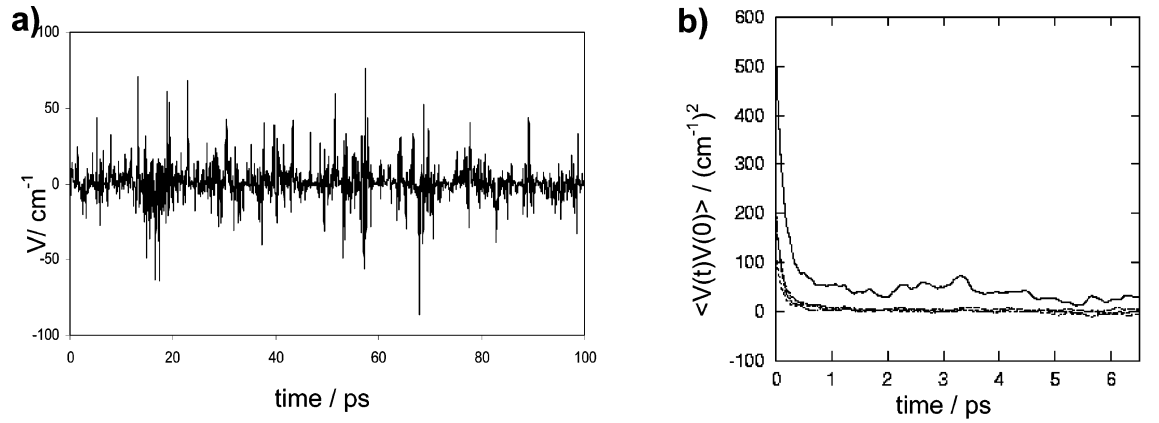

Figure 3. (a) $V^{CS}(t)$ for a portion of trajectory II. $V^{CR}(t)$ shows a similar behavior, but its average value is 4.2 cm^{-1} instead of 0 cm^{-1}. (b) Coupling autocorrelation functions from the CR trajectories (IV (solid)) and from the CS trajectories (I (dashed), II (short dashed), and III (dotted)); the last three are overlapped.

separated D+−A− molecule to compute V^{CR}. Rigorously, the coupling should be computed only at the crossing between the initial and final state potential energy surfaces (PES), whereas we compute it in the vicinity of the initial state minimum. From Hammond's postulate[69] (or assuming a parabolic shape of the PES), the transition state for an exothermic reaction is closer to the initial state minimum than to the final state minimum, and this is the rationale for our choice. To test this approximation's validity, we computed V^{CS} using an MD trajectory for the charge-separated state and computed V^{CR} using an MD trajectory of the neutral state (results omitted). The resulting couplings are only slightly different from the results reported here, which validates this approximation.

3. Results and Discussion

The shorter simulations I−IV with more frequent QC evaluation of the coupling were used to study the time scale of the electronic coupling fluctuation at various temperatures, while the longer simulations V and VI allowed a more accurate evaluation of the average values. For simplicity we first discuss the time scale issue with the assumption that only the closest solvent molecule S can induce coupling between the donor and acceptor.

Characterization of Fluctuations and Effect on the CT Rate. Figure 3a shows the pattern of the couplings $V^{CS}(t)$ for a portion of trajectory II (similar patterns are found in the other simulations). The coupling undergoes extremely large fluctuations that can be properly characterized by the coupling autocorrelation function $\langle V(t)V(0)\rangle$ plotted in Figure 3b for simulations I−IV. This function coincides with the average of the squared coupling $\langle V^2\rangle$ at $t = 0$, and it tends toward $\langle V\rangle^2$ for $t\rightarrow\infty$.[70] The long time value of this function oscillates around its limiting value as a consequence of numerical averaging error. The ratio $\langle V\rangle^2/\langle V^2\rangle$, sometimes called the *coherence parameter*, quantifies the amplitude of the fluctuations. The selection rules of the CS and CR processes are well evident in Figure 3b: for the symmetry-forbidden CS process, the autocorrelation function tends toward zero for $t\rightarrow\infty$, while it tends toward a finite number for the symmetry-allowed CR process. More importantly, the autocorrelation plot in Figure 3b provides information on the time scale of the coupling fluctuation. Regardless of the temperature or the kind of coupling (CS or CR), the system is randomized within a few picoseconds.

Experimental CT rate data are usually fit to expressions derived under the assumption that the coupling is constant even when the system undergoes large geometric fluctuations that affect the coupling. Recently, Troisi et al.[48] showed that the rate constant for CT through fluctuating bridges can be expressed as a series of terms of decreasing importance

$$k = k^{(0)} + k^{(1)} + k^{(2)} + \ldots \tag{7}$$

where the leading term is the rate constant in the static limit

$$k^{(0)} = \frac{2\pi}{\hbar}\langle V^2\rangle\rho_{FCT} \tag{8}$$

In eq 8, ρ_{FCT} is the Franck−Condon and temperature-weighted density of states and $\langle V^2\rangle$ is the average of the squared electronic coupling between donor and acceptor. The static expression in the limit of one classical accepting mode (usually associated with the solvent polarization mode) coincides with the well-known Marcus equation with the squared coupling term substituted by its average value:

$$k^{(0)} = \frac{\langle V^2\rangle}{\hbar}\sqrt{\frac{\pi}{\lambda k_B T}}\exp\left(-\frac{(\lambda + \Delta E^0)^2}{4\lambda k_B T}\right) \tag{9}$$

where λ, $\Delta E°$, and T are, respectively, the reorganization energy, the energy difference between the initial and final states, and the temperature. When the bridge motions can be considered classical, the first non-zero correction term is $k^{(2)}$ and may be expressed as:

$$k^{(2)} = k^{(0)}2\frac{\hbar^2}{\tau_c^2}\left[\frac{(\lambda + \Delta E^0)^2 - 2\lambda k_B T}{(4\lambda k_B T)^2}\right]\left(1 - \frac{\langle V\rangle^2}{\langle V^2\rangle}\right) \tag{10}$$

This correction depends on the potential energy parameters (λ,$\Delta E°$), the coherence parameter $\langle V\rangle^2/\langle V^2\rangle$, and an effective

(69) Hammond, G. S. *J. Am. Chem. Soc.* **1955**, *77*, 334.
(70) Autocorrelation function can be evaluated only if the sign of $V(t)$ is computed consistently. The sign of $V(t)$ depends on the sign of the DA orbitals involved in the CT and is arbitrary. However, once assigned it should not change. We used an ad hoc algorithm that locks the sign of the orbital to its value at $t = 0$. Using this algorithm, the TS component for the symmetry-allowed CR coupling always has the same sign. This is the main cause of the non-zero value of the $\langle V\rangle$ for the CR process. Moreover, the coupling produced by a solvent molecule placed in two mirror symmetric positions is identical for the CR case (leading to $\langle V\rangle \neq 0$) and opposite in sign for the symmetry-forbidden CS process (leading to $\langle V\rangle = 0$).

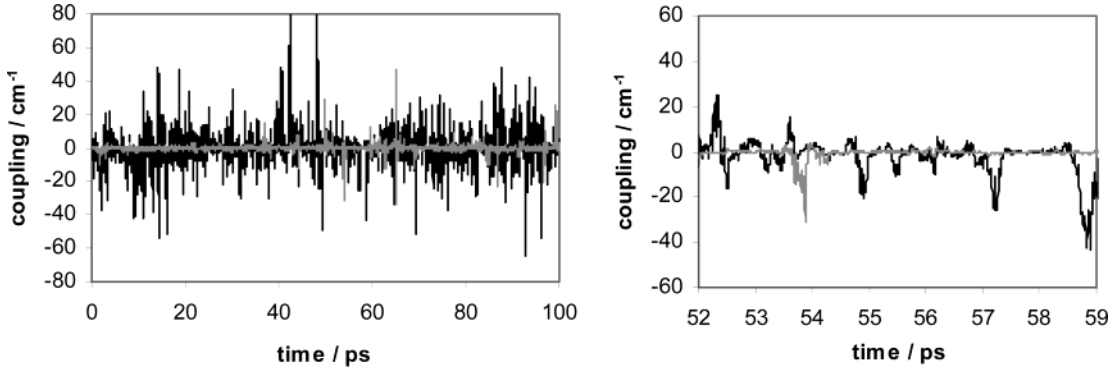

Figure 4. (Left) Time-dependent effective D−A coupling induced by the MeCN solvent molecule closest to the cavity center (black) and by the second closest solvent molecule (gray), computed from a portion of simulation V. (Right) Expanded portion of the same MD trajectory showing that the peaks are due at most to one solvent molecule.

correlation time τ_c.[71] The latter is related to the width of the function $\langle V(t)V(0)\rangle - \langle V\rangle^2$ and measures how fast the coupling changes with time. The advantage of this theoretical formulation is that the validity of a rate constant analysis performed with static limit equations such as eq 9 can be assessed readily through the computation of the correction term in eq 10.

For the CS in MeCN, $\langle V\rangle^2/\langle V^2\rangle = 0$, $\lambda = 0.833$ eV, $\Delta E° = -0.55$ eV (from Table 2, ref 41), and a lower limit for τ_c is 0.1 ps at all the considered temperatures. Using these values, the correction $k^{(2)}$ is 0.04% of $k^{(0)}$ and can be safely ignored. We note that the fastest CT rate observed for A9DME in any solvent is less than 50 ns^{-1},[37] so that solvent motions inside the clamp are fast enough to be averaged during each CT experimental observation and the phenomenon of conformational gating is not observed. On the other hand, the solvent motions are not fast enough to alter the static picture of eqs 8 and 9, i.e., nuclear and electronic motions can be considered effectively uncoupled.

Role of Multiple Solvent Molecules. Figure 4 shows the coupling induced by the first and the second closest molecule (see also Figure 2) in a portion of simulation V. The rms values of the coupling induced by S and S′ are, respectively, 10.1 and 2.77 cm^{-1}, confirming the validity of the geometric criterion used to identify the solvent most effective at inducing coupling. Inspection of the coupling variations shows that only one solvent molecule (usually S) induces a strong coupling at any particular time. Therefore, *interference* between paths through different molecules is not important for this system. In the subsequent analyses we will refer to $V^{CS}(t)$, $V^{CR}(t)$, and their averages, implying that at any given time t we considered the solvent molecule with the largest effective coupling in absolute value. It is worth noting that the computed trajectories do not produce significant time intervals during which the cavity of A9DME is void of solvent.

Role of the Solvent Orbitals. The values of V^{rms} resulting from trajectories V−VIII are collected in Table 3. $V_{TOT}{}^{rms}$, computed using the solvent orbitals listed in Table 1, is the simulation quantity that should most closely correspond to the experimentally fitted coupling. The computed values of $V_{TOT}{}^{rms}$ are between 1.5 and 2 times larger than the experimental estimates, an agreement that is more than satisfactory considering the approximations included in both the computational and fitting procedures. The couplings induced by all three solvents lie within a relatively small range, despite the large differences in the electronic and geometric structures of the solvents.

Table 3. Calculated Rms Couplings (cm^{-1}) from the Simulations[a]

	charge separation coupling			charge recombination coupling
	MeCN	benzene	1,3-DIB	MeCN
V_{TOT}	10.35	9.17	6.03	20.7
V_{FRONT}	6.92	6.37	(0.77)	17.8
V_{HOMO}	4.61	4.00		15.4
V_{LUMO}	5.38	4.13		6.36
V_{TS}	0.681	0.787	0.51	2.65

[a] V_{TOT} employs all the solvent orbitals listed in Table 1. V_{FRONT} employs only the frontier orbitals. V_{HOMO} and V_{LUMO} include only the indicated orbitals of the bridging solvent molecule. V_{TS} is the through-space contribution.

To investigate the contributions of the various *solvent* orbitals in mediating coupling, we computed the (rms) effective coupling induced only by the HOMOs ($V_{HOMO}{}^{rms}$), only by the LUMOs ($V_{LUMO}{}^{rms}$), and by the four frontier orbitals ($V_{FRONT}{}^{rms}$), i.e., HOMOs and LUMOs (the three solvents considered have two degenerate or quasidegenerate HOMOs and LUMOs). We also computed the pure through-space (TS) coupling $V_{TS}{}^{rms}$, i.e., the coupling without mediation by solvent molecules (Table 3). For MeCN (CS and CR) and benzene solvents (CS), the frontier orbitals provide a large fraction of the coupling, as often assumed, but the contribution of the other orbitals (roughly equal to $\sqrt{V_{TOT}{}^{rms^2} - V_{FRONT}{}^{rms^2}}$) is of the same order of magnitude. The HOMOs and LUMOs of MeCN and benzene contribute equally to the coupling for the CS process, while the HOMOs of MeCN are mainly responsible for the coupling in the CR process. The increased importance of the HOMO in CR is related to the lower value of the tunneling energy in the CR process (see Table 1).

A completely different situation is found for the CS process in 1,3-DIB solvent. The frontier orbitals do not contribute to the coupling, which is therefore lower than in the other cases. Inspection of snapshots from this MD trajectory reveals that the 1,3-DIB solvent molecule preferentially accommodates the isopropyl unit inside the clamp as shown in Figure 5, making the frontier orbitals on the aryl fragment ineffective at mediating

(71) Analysis of Figure 3b reveals that more than one characteristic time is involved in the decay of $\langle V(t)V(0)\rangle$. The fastest component is ~0.1 ps. Further investigation of the slower component is omitted because it is not relevant for the experimentally accessible quantities. High-frequency motions (i.e., vibrations of A9DME) do not modulate the coupling significantly because bond-mediated coupling is small in this system.

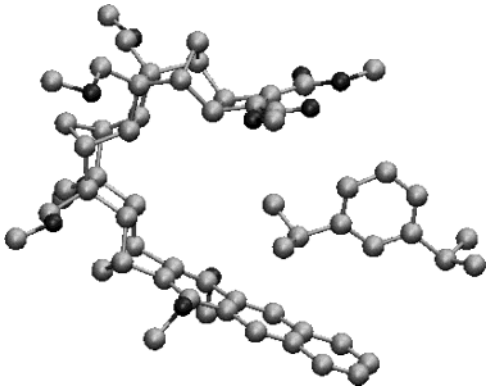

Figure 5. MD snapshot of A9DME in 1,3-DIB, showing the preferred conformation with the isopropyl group inside the clamp.

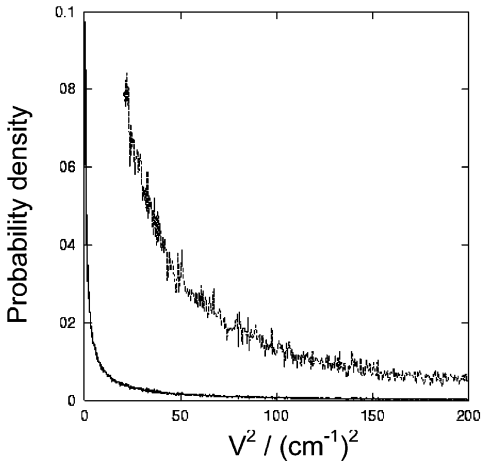

Figure 6. Probability distribution of V^2 obtained from simulation V. The dotted line is the expansion ($\times 20$) of the tail of the distribution.

charge transfer.[72] This arrangement is probably dictated by a more favorable solvent−solvent interaction, since there is in principle enough room for the aromatic ring inside the clamp.

In MeCN, TS coupling for the CR process is substantially larger than for the CS process. The former is formally allowed, while the latter is formally forbidden in the idealized C_s symmetry. However, the TS contribution is so small with respect to the symmetry-breaking solvent-mediated coupling that the selection rules cannot be applied to the overall rate, not even as propensity rules.

The previous considerations imply that the averaging error associated with the computation of $\langle V^2 \rangle$ is small, an assumption that requires further investigation. In Figure 6 we plot the probability distribution of V^2 computed for simulation V. The distribution has a sharp peak at 0 cm^{-1}, and the average is largely determined by the tail of the distribution. A standard deviation cannot be associated directly with the non-Gaussian distribution in Figure 6. Instead, we computed $\langle V^2 \rangle$ for 50 separate portions (20 ps each) of simulation V that can be considered "independent measurements" of $\langle V^2 \rangle$. These values of $\langle V^2 \rangle$ are normally distributed around their average value $(10.351)^2$ $(cm^{-1})^2$ with a standard deviation $\sigma = (6.86)^2$ $(cm^{-1})^2$. We therefore estimate the error of the global average as $2\sigma/\sqrt{50} = (3.66)^2(cm^{-1})^2$ corresponding to an estimated error of the rms value of 0.65 cm^{-1}. A conformational sampling based on short MD can give poor results, especially when the difference of V^{rms} among various systems is being discussed. In our case, the coupling at various temperatures (trajectories I−III) has not produced a statistically meaningful temperature dependence of the rms coupling, a possibility suggested by a recent analysis.[34] A more targeted computational investigation may be required.

Coupling Path Interferences. It is interesting to discuss the contributions of the individual solvent orbitals to the effective coupling. Different paths through different orbitals of the same solvent molecule can interfere constructively or destructively. It is easy to verify numerically that $V_{HOMO}(t) + V_{LUMO}(t) \approx V_{FRONT}(t)$ (see Figure 7a). At a given time, V_{HOMO} and V_{LUMO} can contribute to V_{FRONT} with the same sign (constructive interference) or the opposite sign (destructive interference), as shown in Figure 7b,c. Although the solvent HOMO and LUMO make comparable contributions to the coupling when an entire trajectory is considered, their individual contributions for specific solvent configuration do not appear to be correlated.

Relative Importance of Occupied and Virtual Solvent Orbitals. It is difficult to interpret confidently the variation of coupling with solvent given the active role of many mediating orbitals, the often unpredictable solvent configurations around the solute, and the possible effects of interference. For the 17 solvents in which A9DME was studied experimentally,[40] the solvent property that exhibited the best correlation with the electronic coupling was vertical electron affinity. This was interpreted as indicating that coupling pathways involving the solvent LUMO dominate the donor−acceptor interaction. However, the results in Table 3 indicate substantial coupling involving filled orbitals. To probe the origin of the experimental correlation between coupling and electron affinity, we performed the following numerical experiment: the energy of the solvent virtual orbitals or, alternatively, the energy of the occupied solvent orbitals was shifted and the coupling recalculated in order to visualize the influence of solvent levels on the coupling while leaving every other factor (solvent structure and positioning, orbital shapes, etc.) unchanged. We used the trajectory with benzene as the solvent (VII) to compute the sensitivity of the CS coupling to the energies of the virtual and occupied solvent orbitals (Figure 8). The effective coupling increases when the occupied orbitals are shifted upward in energy or the virtual orbitals are shifted downward (as expected), but the coupling is far more sensitive to the position of the solvent virtual orbitals (this is due to their closer proximity to E_{tunn}). According to these calculations, decreasing the virtual orbital energy by 1.4 eV increases the rms coupling by 42%. The experimental value of CS coupling in benzonitrile (with an electron affinity 1.4 eV lower than benzene) is actually 60% higher than the value observed in benzene.[41,73] The calculations provide theoretical support for the experimentally observed correlation between the coupling magnitude for A9DME and solvent LUMO energies. At the same time, the calculations point to significant, but weakly solvent-dependent, contributions to the coupling from occupied solvent orbitals. This example shows once more how

(72) We checked that our finding was not due to incomplete sampling of the configurational space by performing repeated simulated annealing from 1000 K. Even when the aryl portion is initially forced into the cavity, the system relaxes to a configuration similar to that of Figure 5. An additional difference with respect to the MeCN and benzene solvent is that the 1,3-DIB molecules are less mobile inside the clamp.

(73) The 1.4 eV decrease in the LUMO from C_6H_6 to C_7H_5N is accompanied by a decrease in the HOMO energy of only 0.5 eV.

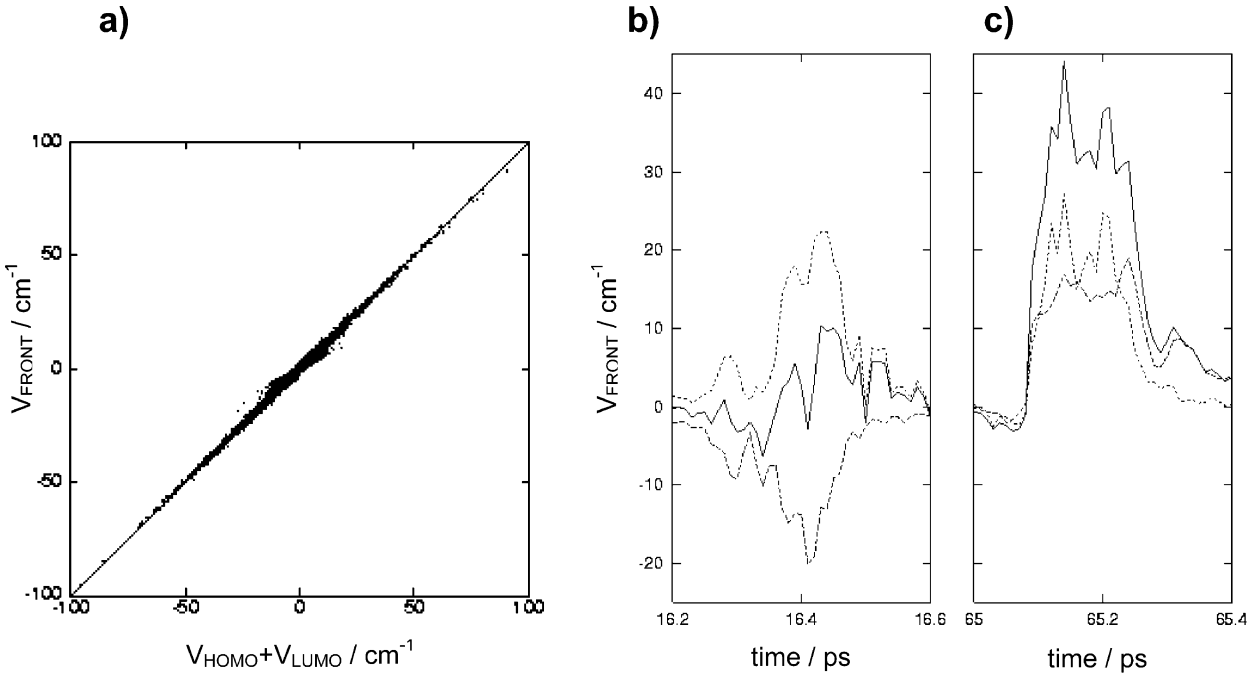

Figure 7. (a) Verification of the relation $V_{HOMO} + V_{LUMO} \approx V_{FRONT}$ using the computed values from trajectory IV. Example of destructive (b) and constructive (c) interference in two portions of the same trajectory: $V_{FRONT}(t)$ (solid line), $V_{HOMO}(t)$ (dashed line), $V_{LUMO}(t)$ (dotted line).

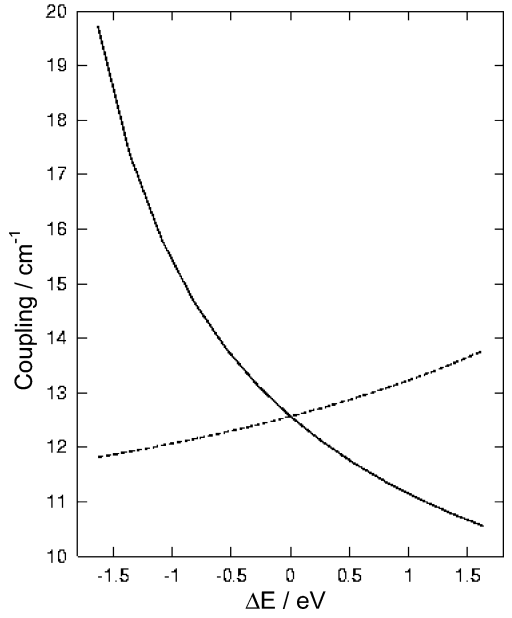

Figure 8. Effect on V_{TOT}^{rms} (simulation VII with benzene) of shifting the virtual orbitals (solid line) or the occupied orbitals (dashed line) of the solvent by ΔE. The coupling is more sensitive to shifts of the virtual orbitals.

numerical experiments, made possible by molecular modeling techniques, can isolate the effect of an individual parameter on the global rate constant.

Solvent Configurations with High Coupling. The large coupling fluctuations observed in the simulations indicate a complicated dependence of electronic coupling on the solvent configuration that, presumably, reflects the overlap between the complex shapes of the D, A, and S orbitals.[41] The prior discussions demonstrated that a minority of trajectory points are the primary sources of the electronic coupling. An attempt was made to characterize these high coupling configurations for the CR process.

It was not possible to rationalize the peaks in the $V^{CR}(t)$ function by simple inspection of the corresponding snapshots. To visualize the solvent configurations leading to peak coupling, we define a reference system as outlined in Figure 9a. Three auxiliary points are defined: O is the center of mass of the six-member aromatic ring of the donor connected to the bridge, P is the center of mass of the terminal six-member aromatic ring of the donor, and Q is the center of mass of the cyclobutene acceptor ring. O defines the origin, and the Cartesian axes are oriented so that P is on the *z* axis and Q is on the *xz* plane (with this reference system, the system is observed from the point of view of the donor). We considered 10 000 snapshots of trajectory VI (one every 0.1 ps) and represented the MeCN solvent with an arrow pointing from the central carbon atom toward the nitrogen atom. In this way it is possible to achieve a global view of the solvent positions that most effectively mediate the coupling. Figures 9b−d represent the *xy*, *xz*, and *yz* projections of the system; the solvent position was represented only if $|V^{CR}| > 35$ cm^{-1} (6.9% of the trajectory points are above this threshold). Figure 9e is similar to Figure 9d, but the threshold was set to 75 cm^{-1} (1.2% of trajectory points). For simplicity, only the *average* position of several DA atoms is shown; in fact, the clamp undergoes deformations that explain the presence of arrows apparently outside the cavity (the average distance between points O and P during the simulation was 6.3 Å with standard deviation 0.3 Å).

While Figures 9b,c clearly reflect the requirement that a solvent molecule lie in the cavity in order to mediate the coupling, Figures 9de are best suited to examine correlations between solvent placement, electronic structure, and coupling magnitude. Figure 10 displays the orbitals φ_{DH} and φ_{AL} involved in the charge recombination process. A solvent can mediate the coupling only if its orbitals overlap simultaneously with φ_{DH} and φ_{AL}. Figure 9d is reminiscent of the φ_{DH} orbital, with the two central lobes on the anthracene fragment appearing as the positions most densely populated by high coupling configura-

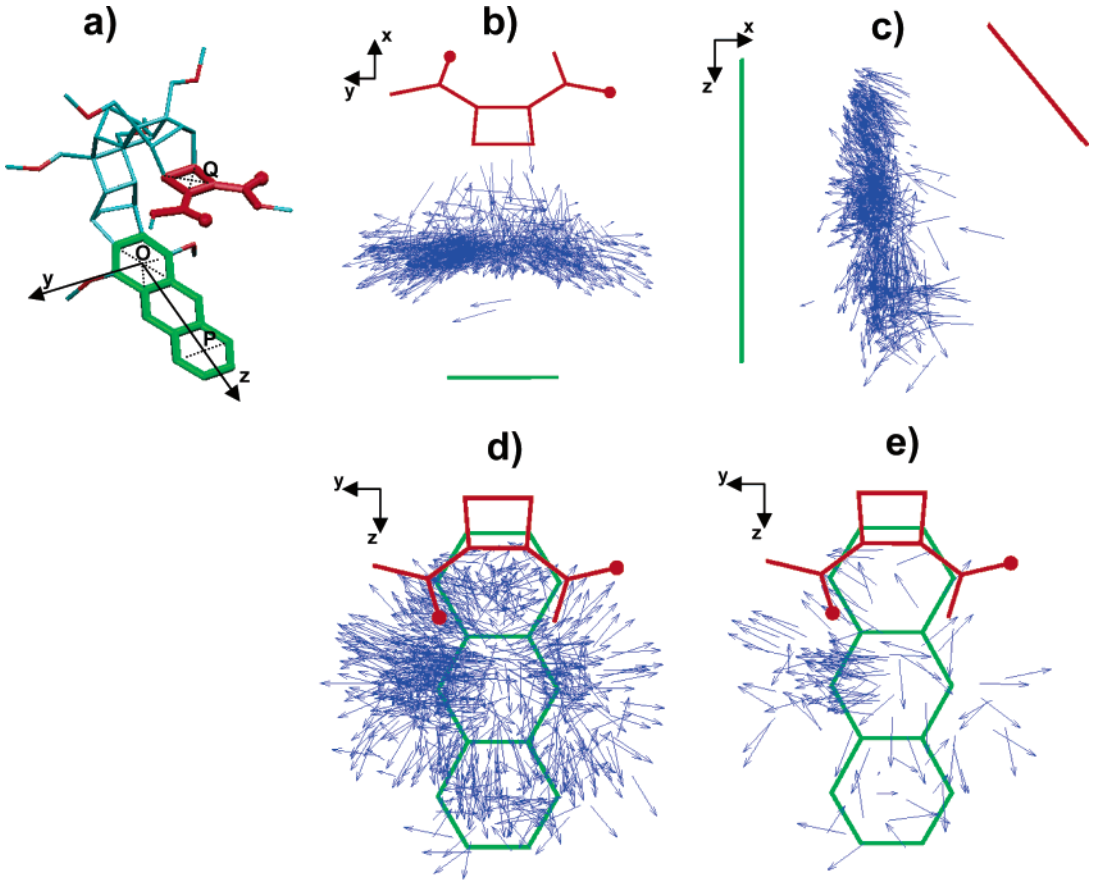

Figure 9. (a) Definition of the reference system. Positions of the MeCN molecules when $|V^{CR}|$ is above 35 cm^{-1} projected on the planes *xy* (b), *xz* (c), and *yz* (d). The average position of several DA atoms is outlined. (e) *yz* projection limited to the solvent position with coupling higher than 75 cm^{-1}. The full circles in (bde) identify the carbonyl oxygens.

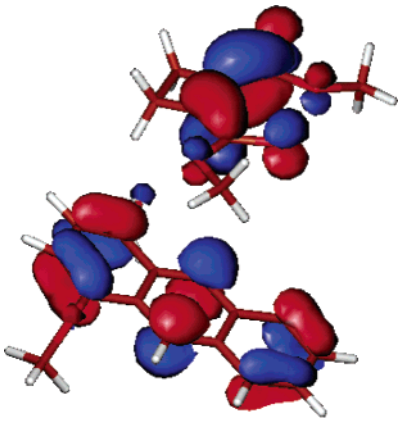

Figure 10. Shape of the φ_{DH} and φ_{AL} orbitals involved in the CR process.

tions. The central lobes of φ_{DH} are in closest proximity to φ_{AL} and therefore more likely to be involved in the coupling. The nodal plane common to the two orbitals is responsible for the lower probability of finding a high coupling configuration when a solvent is centrally located in the cavity. The asymmetry in Figures 9d and 9e (particularly evident in the latter) is induced by the asymmetric configuration of the carbonyl groups in the acceptor. Since the carbonyl makes a substantial contribution to the φ_{AL} orbital, a higher coupling configuration is more probable on the side where the carbonyl points toward the center of the cavity. In a majority of the high coupling configurations, the solvent is oriented with its methyl group in the hydrophobic center of the cavity.

Identifying structure−coupling correlations from the simulations becomes increasingly difficult when the larger solvent molecules are involved (e.g., benzene). While the global effect of the solvent is to lower the tunneling barrier, many paths differing electronically and geometrically contribute.

4. Conclusions

In this paper we combined MD simulations of a C-clamp molecule in different solvents with the QC evaluation of the electronic coupling relevant for the CT reactions. We characterized the amplitude and the time scale of the electronic coupling fluctuations for the charge separation and charge recombination processes, considering the consequences of this fluctuating behavior on the observed rate constant. Overall, the characteristic time scale for fluctuation of the coupling is ∼0.1 ps. This time scale is too slow to introduce significant corrections to the rate expressions based in the Condon approximation. On the other hand, this time scale is too fast to develop inhomogeneity in the observed transfer rate constants. The conventional Marcus-like expression can be used to an excellent level of approximation if the fitted value of the coupling is interpreted as a root-mean-square average over the solvent configurations. The reliable evaluation of this average from MD simulations is not trivial since a minority of trajectory points gives the largest contribution to the coupling. We suggest that an extensive conformational sampling for systems with fluctuating coupling is at least as important as the accuracy in the computation of coupling in a single conformation. These simulations of A9DME

rule out the possibility of specific interference effects between multiple molecules mediating the coupling but reveal that paths through different orbitals of the same solvent molecule may interfere. We quantified the role of the different solvent orbitals in mediating the CT, verifying that one has to include a large number of them to avoid misleading results. The effective coupling induced by the solvent depends on a large number of factors whose overall outcome is hard to predict. We verified that the coupling magnitude for the charge separation is most sensitive to the energy of the virtual orbitals, as suggested by the analysis of a large body of experimental results, but that coupling is also significantly mediated by filled orbitals in many solvents. We found that the distribution of solvent molecules in high coupling configurations is reminiscent of the shape of the D/A orbitals involved in the coupling.

The results presented here demonstrate the usefulness of a MD/QC study in disentangling the many aspects of CT in nonrigid systems. While the Marcus-like formula is semiquantitatively correct if the appropriate (multiorbital and geometrically averaged) value of V^2 is used, the process is dynamical at many levels, sampling both coupling and geometric spaces very extensively. This suggests that experiments involving single-molecule decay measurement analogues to single-molecule spectroscopies[74] would be very helpful in sorting out the details that contribute to the kinetics measurement.

Acknowledgment. Work of A.T. and M.R. was supported by the Chemistry Divisions of the NSF and the ONR and by the MURI/DURINT program of the DOD. Work of M.B.Z. was supported by the NSF (CHE-0108945).

JA038905A

(74) (a) Jung, Y.; Barkai, E.; Silbey, R. J. *Adv. Chem. Phys.* **2002**, *123*, 199. (b) Moerner, W. E.; Orrit, M. *Science* **1999**, *283*, 1670. (c) Xie, X. S.; Trautman, J. K. *Ann. Rev. Phys. Chem.* **1998**, *49*, 441.